

# The Zak phase and the existence of edge states in graphene

P. Delplace

*Département de Physique Théorique, Université de Genève, CH-1211 Genève, Switzerland*

D. Ullmo

*Laboratoire de Physique Théorique et Modèles Statistiques,  
CNRS UMR 8626, Univ. Paris-Sud, 91405 Orsay Cedex, France*

G. Montambaux

*Laboratoire de Physique des Solides, CNRS UMR 8502, Univ. Paris-Sud, 91405 Orsay Cedex, France*

We develop a method to predict the existence of edge states in graphene ribbons for a large class of boundaries. This approach is based on the bulk-edge correspondence between the quantized value of the Zak phase  $\mathcal{Z}(k_{\parallel})$ , which is a Berry phase across an appropriately chosen one dimensional Brillouin zone, and the existence of a localized state of momentum  $k_{\parallel}$  at the boundary of the ribbon. This bulk-edge correspondence is rigorously demonstrated for a one dimensional toy model as well as for graphene ribbons with zigzag edges. The range of  $k_{\parallel}$  for which edge states exist in a graphene ribbon is then calculated for arbitrary orientations of the edges. Finally, we show that the introduction of an anisotropy leads to a topological transition in terms of the Zak phase, which modifies the localization properties at the edges. Our approach gives a new geometrical understanding of edge states, it confirms and generalizes the results of several previous works.

## I. INTRODUCTION

The physics of edge states in two-dimensional (2D) systems has emerged as a very challenging problem in solid state physics. A beautiful illustration occurs in graphene, a monolayer crystal of carbon,<sup>1</sup> where the existence of such states was predicted<sup>2,3</sup> in 1996 and confirmed experimentally later in graphene<sup>4,5</sup> and graphene-like structures.<sup>6</sup> This remarkable feature led to a strong activity during the last few years. For instance, edge states were predicted to give rise to a novel type of magnetic ordering<sup>2</sup> and may lead to the realization of novel spintronic devices.<sup>7,8</sup>

In a broader context, edge states are also known to play an important role in quantum Hall systems<sup>9,10</sup> and topological insulators.<sup>11,12</sup> Because of their chiral character, the edge states in quantum Hall systems are robust against all kind of disorder or interactions, while those in topological insulators survive scattering that preserves the time reversal symmetry. This robustness against weak perturbations can be understood from a correspondence between the number of edge states and the value of a bulk topological number which is basically the Berry curvature integrated over the space of parameters, that is the Brillouin zone of the 2D system<sup>12,13</sup>.

Edge states in graphene differ from those mentioned above, the most important distinction being that their existence depends on the boundary conditions fixed by the shape of the edge<sup>2,3</sup>. Then, two questions naturally arise. The first one is related to the bulk-edge correspondence:<sup>14-17</sup> if the localization of a state at the edge depends on the boundaries, is it possible to relate its existence to a topological quantity defined within the bulk? The second question is simply whether we can predict the existence of edge states for an arbitrary type of edge (see e.g. some examples on Fig. 1).

These two stimulating questions have already led to many works. In particular, Ryu and Hatsugai showed that edge states in 2D systems with chiral symmetry can be related to a bulk topological number defined in a reduced (1D) space of parameters.<sup>14</sup> More precisely, these authors were able to characterize edge states for three simple types of boundaries, namely the zigzag, armchair and bearded edges (a bearded edge is a zigzag edge with dangling bonds, also called Klein

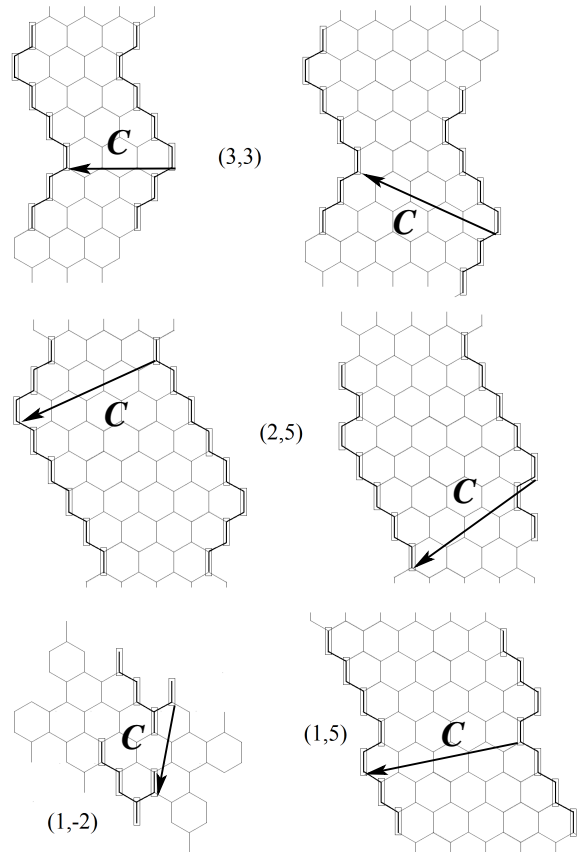


FIG. 1. Examples of edges of different ribbons studied in this paper. They are characterized by a translation vector  $\mathbf{T}(m, n)$ , see section III B. The values of the couples  $(m, n)$  are specified in the figure. The edges of the ribbon  $(1, -2)$  shows dangling bounds since  $mn < 0$ . Different ribbons can be obtained from the same vector  $\mathbf{T}(m, n)$  in two different ways. For instance, the lattice vectors  $\mathbf{C}$  connecting the left and right edges of the two ribbons defined by  $\mathbf{T}(3, 3)$  are different. An other possibility is to draw a different “unit-cell” pattern for the same vector  $\mathbf{T}$ , as for the two ribbons defined by  $\mathbf{T}(2, 5)$ .

defects<sup>18,19</sup>). Of course, even without disorder, there is an infinite number of different edge geometries in a honeycomb lattice, and several recent theoretical works addressed the existence of edge states for more sophisticated boundaries. Several of these works consist in tight-binding calculations of ribbons band structures.<sup>2,3,20–22</sup> A general study including many various shapes of edges was also achieved by Akhmerov and Beenakker.<sup>23</sup> This work, performed within the continuous (Dirac) approximation, notably provides an analytical formula for the density of edge states.

The aim of this work is to precise the bulk-edge correspondence in graphene and to address a new method to predict the existence of edge states for a large class of edges. We show that it is possible to define in an unambiguous way a topological phase from the bulk Hamiltonian of graphene, which properly takes into account the shape of the edges. For a 1D system, this phase, called Zak phase, is nothing but the integration of the Berry connection over the first Brillouin zone<sup>24</sup>

$$\mathcal{Z} = i \oint dq \langle u_q | \partial_q u_q \rangle, \quad (1)$$

where the  $|u_q\rangle$  are the Bloch wave functions. In a 2D system, one difficulty is to define properly the path over which the integration is performed, and to relate this quantity to the nature of the edge. In particular, for a translation invariant system in one direction, the Zak phase depends on the crystal momentum  $k_{\parallel}$  associated with this direction. Here, we show that  $\mathcal{Z}(k_{\parallel})/\pi$  gives the number of states localized at the edge of the system.

The outline of the paper is as follows. As the Zak phase is defined as a one-dimensional integral of the Berry connection, we first focus in Sec. II on a one-dimensional toy model for a chain of dimers. For this case, we give a simple demonstration of the bulk-edge correspondence between the Zak phase and the existence of edge states. Next, in Sec. III, we turn to graphene where a similar demonstration is performed for zigzag edges. By a formal analogy with the chain of dimers, we assume the generalization of this bulk-edge correspondence for the other boundaries. Then, we show how to define in an unambiguous way the Zak phase in graphene according to the nature of the edge and propose a very simple graphical method to evaluate it. This information then directly gives us the range of  $k_{\parallel}$  for which edge states exist. The analytical results are in perfect agreement with those of Akhmerov and Beenakker<sup>23</sup> and reproduce many numerical works. Finally, in Sec IV we extend our approach by considering non-equal hopping parameters in the honeycomb lattice. We discuss the existence of edge states in this case and explain recent numerical calculations in terms of the Zak phase.<sup>25</sup>

## II. THE ZAK PHASE AND THE EDGE STATES IN THE CHAIN OF DIMERS

To illustrate the relation between the Zak phase and boundary states, we consider in this section a simple model, a one-dimensional chain of dimers  $A$ - $B$  as shown in Fig. 2. The two atoms of the dimers are coupled by a hopping parameter  $t'$  and the chain is obtained by coupling periodically the dimers with a hopping parameter  $t$ . The lattice spacing (between two consecutive identical atoms) is  $a_0$ .

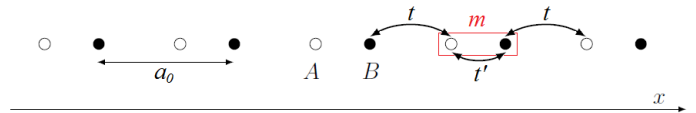


FIG. 2. Chain of dimers  $A$ - $B$ . The chain starts with an atom  $A$  and ends with an atom  $B$ .  $t$  and  $t'$  are the hopping parameters and  $a_0$  is the lattice spacing. The unit cell  $m$  is represented by a rectangle.

The aim of this section is to show in a simple way that the Zak phase  $\mathcal{Z}$  is governed by the ratio  $t'/t$ , and that the topological transition ( $\mathcal{Z}=0$ )  $\rightarrow$  ( $\mathcal{Z}=\pi$ ) corresponds to the emergence of edge states in the finite system.

### A. The bulk Hamiltonian

The Hamiltonian of the dimer chain is given by

$$\hat{H} = \sum_{m=1}^M t' b_m^\dagger a_m + t a_{m+1}^\dagger b_m + h.c., \quad (2)$$

where  $a_m^\dagger$  (resp.  $b_m^\dagger$ ) creates a particle on the site  $A$  (resp.  $B$ ) of the  $m^{\text{th}}$  dimer.

For periodic boundary conditions, we can use the Bloch theorem and rewrite  $\hat{H}$  as

$$\hat{H} = \sum_{k_n \equiv \frac{2\pi n}{a_0}} \Psi_{k_n}^\dagger \mathcal{H}^B(k_n) \Psi_{k_n} \quad \left(-\frac{M}{2} < n < \frac{M}{2}\right), \quad (3)$$

with  $\Psi_k^\dagger = (\psi_{A,k}^\dagger, \psi_{B,k}^\dagger) = M^{-1/2} \sum_{m=1}^M e^{ia_0 m k} (a_m^\dagger, b_m^\dagger)$  and

$$\mathcal{H}^B(k) = -t \begin{pmatrix} 0 & \rho(k) \\ \rho^*(k) & 0 \end{pmatrix}, \quad (4)$$

where  $\rho(k) = t'/t + e^{-ika_0}$ . Introducing  $\sigma = (\sigma_x, \sigma_y)$  the vector of Pauli matrices,  $\mathcal{H}^B(k)$  can be expressed in the form

$$\mathcal{H}^B(k) = -t \mathbf{g}(k) \cdot \sigma \quad (5)$$

with  $\mathbf{g}(k) = (\text{Re } \rho, -\text{Im } \rho) = (t'/t + \cos ka_0, \sin ka_0)$ . Diagonalizing  $\mathcal{H}^B(k)$  we obtain the eigenvalues

$$\epsilon_{k,\pm} = \pm t |\mathbf{g}(k)| = \pm t |\rho(k)| = \pm \sqrt{t^2 + t'^2 + 2tt' \cos(ka_0)}, \quad (6)$$

and writing  $\rho(k) = |\rho(k)| e^{-i\phi(k)}$ , we have

$$\mathbf{g}(k) = |\rho(k)| \begin{pmatrix} \cos \phi(k) \\ \sin \phi(k) \end{pmatrix}, \quad (7)$$

with the phase  $\phi(k)$  given by

$$\cot \phi(k) = \frac{t'/t}{\sin ka_0} + \cot ka_0. \quad (8)$$

The winding of the vector  $\mathbf{g}(k)$  as  $k$  varies across the Brillouin zone is shown in Fig. 3 for two values of  $t'/t$ . When  $t'/t > 1$ , the curve  $\mathbf{g}(k)$  does not enclose the origin and  $|\phi(k)| < \pi/2$  for all  $k$ . When  $t'/t < 1$ , the loop encloses the origin and the phase  $\phi(k)$  can take any value. This topological behavior of the phase  $\phi(k)$  is furthermore closely related

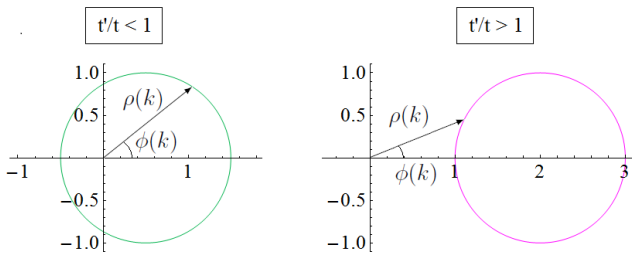


FIG. 3. Two trajectories of the vector  $\mathbf{g}(k)$  with different topologies when  $k$  runs across the Brillouin zone. When  $t'/t < 1$  ( $t'/t > 1$ ) the curve  $\mathbf{g}(k)$  does (not) wind around the origin.

to the value of the Zak phase. Indeed, the eigenvectors of  $\mathcal{H}^B(k)$  are of the form

$$|u_{k,\pm}\rangle = \frac{1}{\sqrt{2}} \begin{pmatrix} e^{-i\phi(k)} \\ \pm 1 \end{pmatrix}, \quad (9)$$

and the definition Eq. (1) of the Zak phase gives

$$\mathcal{Z} = \frac{1}{2} \oint dk \frac{d\phi}{dk} = \frac{\Delta\phi}{2}, \quad (10)$$

where  $\Delta\phi$  is the variation of  $\phi(k)$  when  $k$  varies across the full Brillouin zone. The Zak phase  $\mathcal{Z}$  is  $\pi$  times the winding number of the curve  $\mathbf{g}(k)$  around the origin, and is therefore zero if this curve does not enclose the origin and  $\pi$  if it does. Thus

$$\begin{aligned} \mathcal{Z} &= 0 & \text{when } t'/t > 1 \\ \mathcal{Z} &= \pi & \text{when } t'/t < 1. \end{aligned} \quad (11)$$

Eq. (11) shows that tuning the ratio  $t'/t$  induces a topological transition (at  $t'/t = 1$ ) characterized by the Zak phase  $\mathcal{Z} = 0 \longleftrightarrow \mathcal{Z} = \pi$ .

## B. Open boundary conditions

### 1. The missing bulk states and the Zak phase

Consider now a finite chain of  $M$  dimers with open boundary conditions. We impose that the wave function vanishes at the nearest site outside the chain, that is on the  $B$  site at  $m = 0$  and the  $A$  site at  $m = (M + 1)$ . Most of the eigenvectors can be constructed as linear combinations  $|v_{k,\pm}\rangle$  of the bulk eigenfunctions with opposite momentum  $|u_{k,\pm}\rangle$  and  $|u_{-k,\pm}\rangle$ . Writing  $|u_{k,\pm}\rangle$  as

$$|u_{k,\pm}\rangle = \sqrt{\frac{1}{2M}} \sum_{m=1}^M e^{ika_0 m} \begin{pmatrix} e^{-i\phi(k)} \\ \pm 1 \end{pmatrix} \cdot (|m, A\rangle, |m, B\rangle), \quad (12)$$

where  $|m, A/B\rangle$  denotes the orbital  $A/B$  in the cell  $m$ , we obtain from the condition  $\langle 0, B|v_{k,\pm}\rangle = 0$  that  $|v_{k,\pm}\rangle = \frac{1}{\sqrt{2}} [|u_{k,\pm}\rangle - |u_{-k,\pm}\rangle]$ . Thus, using  $\phi(-k) = -\phi(k)$ , we have

$$|v_{k,\pm}\rangle = \frac{i}{\sqrt{M}} \sum_m \begin{pmatrix} \sin(ka_0 m - \phi(k)) \\ \pm \sin(ka_0 m) \end{pmatrix} \cdot (|m, A\rangle, |m, B\rangle). \quad (13)$$

Finally, the boundary condition  $\langle (M + 1), A|v_{k,\pm}\rangle = 0$  imposes the quantization condition

$$k(M + 1)a_0 - \phi(k) = \kappa\pi, \quad \kappa = 1, \dots, M, \quad (14)$$

which has to be solved in the range  $0 < k < \pi/a_0$  (the wave functions corresponding to  $k = 0$  and  $k = \pi/a_0$  are identically zero). The function  $\phi(k)$  is plotted in Fig. 4, and the solutions of Eq. (14) correspond to the intersection of  $\phi(k)$  with the  $M$  lines  $f_\kappa(k) = (M + 1)ka_0 - \kappa\pi$ .

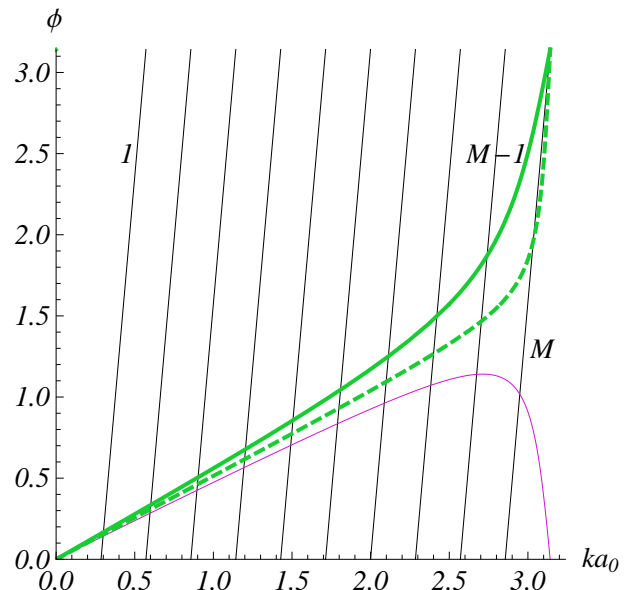


FIG. 4. Variation  $\phi(k)$  for  $t'/t = 1.1$  (bottom curve),  $t'/t = 0.8$  (upper thick curve), and  $t'/t = 0.95$  (thick dashed curve). The straight lines are lines of equation  $f_\kappa(k) = (M + 1)ka_0 - \kappa\pi$ . Here, we have chosen  $M = 10$ , for which  $(t'/t)_c = 0.9091$ . The extreme values of  $\kappa$  are indicated on the figure. In the latter case  $t'/t = 0.95 > (t'/t)_c$ , so that there are  $M$  bulk states although the Zak phase  $\mathcal{Z} = \pi$ .

From this figure, we see that the Zak phase controls the number of bulk states and therefore the existence of edge states. Indeed, when  $t' > t$ ,  $\phi(\pi/a_0) = 0$  and Eq. (14) has  $M$  solutions. When  $t' < t$ ,  $\phi(\pi/a_0) = \pi$  and in this case there are  $M$  or  $M - 1$  solutions depending on the value of  $t'/t$ . By comparing the slopes of the curves  $\phi(k)$  and  $f_M(k)$ , we immediately obtain that the number of bulk states  $|v_{k,\pm}\rangle$  depends on the critical value of the ratio  $t'/t$

$$\left(\frac{t'}{t}\right)_c = 1 - \frac{1}{M + 1}. \quad (15)$$

Including the factor 2 associated with negative and positive energies for each solution of the quantization condition (14), the number  $N_{\text{bulk}}$  of bulk states is:

$$\begin{aligned} N_{\text{bulk}} &= 2M & \text{when } t'/t > (t'/t)_c \\ N_{\text{bulk}} &= 2(M - 1) & \text{when } t'/t < (t'/t)_c. \end{aligned} \quad (16)$$

As we show below, the missing states are edge states localized at the ends of the chain. In the large  $M$  limit, the number of bulk states is related to the value of  $\phi(\pi/a_0)$  since, in this limit, there are  $2M$  bulk solutions when  $\phi(\pi/a) = 0$  and  $2(M - 1)$  bulk solutions when  $\phi(\pi/a) = \pi$ . This criterion can be rewritten in terms of the Zak phase: since  $\phi(k)$  is an odd function of  $k$ , we have simply

$$\mathcal{Z} = \frac{1}{2} \oint dk \frac{d\phi}{dk} = \int_0^{\pi/a_0} dk \frac{d\phi}{dk} = \phi(\pi/a_0) = 0 \text{ or } \pi \quad (17)$$

As a result, by comparing Eqs. (11), (15) and (16), we conclude that in the large  $M$  limit,<sup>26</sup>

$$\begin{aligned} N_{\text{bulk}} &= 2M && \text{when } \mathcal{Z} = 0 \\ N_{\text{bulk}} &= 2(M-1) && \text{when } \mathcal{Z} = \pi. \end{aligned} \quad (18)$$

## 2. The edge states

We now briefly describe the structure of the edge state for  $t'/t < (t'/t)_c$ . We search for a solution  $k$  of the form  $k = \pi/a_0 + i\lambda$ , where  $\xi = 1/\lambda$  is the localization length of the edge state. The solution vanishing on the  $B$  site at  $m = 0$  is of the form

$$|v_{\lambda,\pm}^e\rangle = \frac{1}{\sqrt{M}} \sum_{m=1}^M (-1)^{m+1} \begin{pmatrix} \chi_m^A \\ \chi_m^B \end{pmatrix} \cdot (|m, A\rangle, |m, B\rangle), \quad (19)$$

where

$$\begin{pmatrix} \chi_m^A \\ \chi_m^B \end{pmatrix} = \begin{pmatrix} \left( \frac{t'}{t} \sinh \lambda a_0 m - \sinh \lambda a_0 (m-1) \right) / |\rho(\lambda)| \\ \pm \sinh \lambda a_0 m \end{pmatrix}, \quad (20)$$

and has an energy

$$\epsilon_{\lambda,\pm} = \pm \sqrt{t^2 + t'^2 - 2tt' \cosh \lambda a_0} \equiv \pm t |\rho(\lambda)|. \quad (21)$$

The inverse localization length  $\lambda$  is fixed by the condition that the wave function on the site  $A$  at  $m = (M+1)$  vanishes, leading to

$$t' \sinh \lambda (M+1) a_0 = t \sinh \lambda M a_0. \quad (22)$$

Inserting (22) into (21), we find

$$\epsilon_{\lambda,\pm} = \pm t \frac{\sinh \lambda a_0}{\sinh \lambda (M+1) a_0}, \quad (23)$$

and the components of the edge states wave functions can be rewritten as

$$\begin{pmatrix} \chi_m^A \\ \chi_m^B \end{pmatrix} = \begin{pmatrix} \sinh \lambda a_0 (M+1-m) \\ \pm \sinh \lambda a_0 m \end{pmatrix}, \quad (24)$$

which satisfy properly the boundary conditions. Far from the transition, that is when the localization length  $\xi$  is much smaller than the size of the chain  $Ma_0$ , Eq. (22) reads

$$\frac{t'}{t} \simeq \exp(-\lambda a_0). \quad (25)$$

This implies  $\cosh(\lambda a_0) \simeq (t^2 + t'^2)/2tt'$ , and thus  $\epsilon_{\lambda,\pm} \simeq 0$ . More precisely, from Eq. (23), the energy vanishes as  $\epsilon_{\lambda,\pm} \simeq \exp(-\lambda M a_0)$ . The dependence  $\lambda(t'/t)$  for a chain of  $M = 10$  dimers is shown in Fig. 5, together with the approximate expression Eq. (25). The energy spectrum of the same chain is displayed in Fig. 6.

## C. Remarks on the chiral symmetry

We finish this section with a few brief remarks concerning the Zak phase and symmetries. As first stressed by Ryu and Hatsugai,<sup>14</sup> the fact that the edge states have zero energy is associated with the existence of a chiral symmetry of

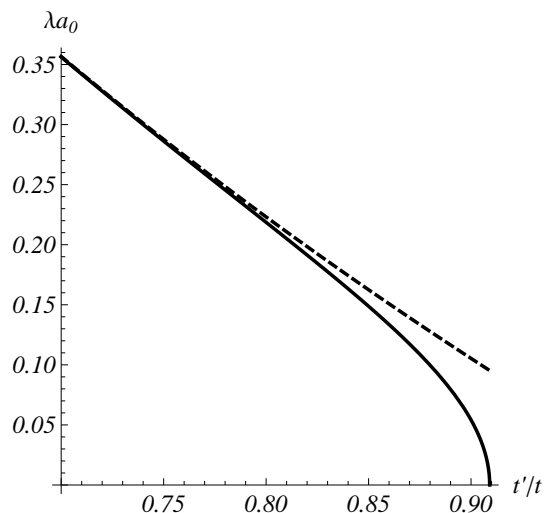


FIG. 5. Inverse localization length  $\lambda$  as a function of the parameter  $t'/t$ , for a chain of  $M = 10$  dimers. The full curve is the solution of Eq. (22). As expected, it diverges as the ratio  $t'/t$  reaches the critical value given by Eq. (15). The dashed line corresponds to the approximation (25) valid far from the transition and corresponding to  $\epsilon = 0$ .

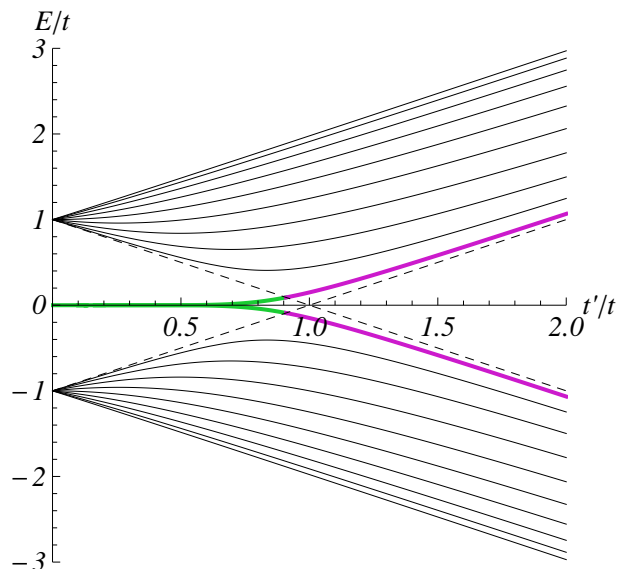


FIG. 6. Energy levels as a function of the parameter  $t'/t$ , for a chain of  $M = 10$  dimers. There is an edge state with an energy close to 0 when  $t'/t < 1 - 1/(1+M)$ . The dashed lines correspond to the gap  $\pm(t' - t)$  in the limit  $M \rightarrow \infty$ . The thick (dark, purple online) curve is the energy of the lowest energy state which becomes an edge state (light, green online) when  $(t'/t)_c < 1$ .

the bulk Hamiltonian.<sup>27</sup> From an algebraic point of view, a chiral symmetry is represented by an operator  $\mathcal{C}$  which anticommutes with the bulk Hamiltonian and which satisfies  $\mathcal{C}^2 = \mathbb{1}$ . As the Bloch Hamiltonian of the chain of dimers can be written as a linear combination of the Pauli matrices  $\sigma_x$  and  $\sigma_y$ , it is clear that  $\mathcal{C} = \sigma_z$  fulfills these properties. Now, we note that the Zak phase measures the solid angle drawn by the pseudo-spinor in the Bloch sphere when  $k$  spans the Brillouin zone. As long as the Hamiltonian does not have a component proportional to  $\sigma_z$ , the pseudo-spinor is forced to evolve on the equator of the Bloch sphere, and the Zak phase is necessarily a multiple of  $\pi$ . We notice that

breaking the inversion symmetry of the chain,<sup>24</sup> for instance by adding a staggered potential, would add a term proportional to  $\sigma_z$  in the Hamiltonian and therefore would break the chiral symmetry. As a consequence, the Zak phase is not expected to be a multiple of  $\pi$  anymore in this case and the energy of the edge states can be different from zero.

Adding a term proportional to the identity trivially breaks the chiral symmetry and shifts the energy while leaving the pseudo-spinor on the equator so that the Zak phase is still quantized as a multiple of  $\pi$ . A configuration where this simple mechanism leads to an interesting physics is obtained by coupling chains of dimers (assumed oriented along the  $x$ -direction) by a hopping parameter  $t''$  along the  $y$  direction, as displayed in Fig. 7. For periodic boundary conditions, the

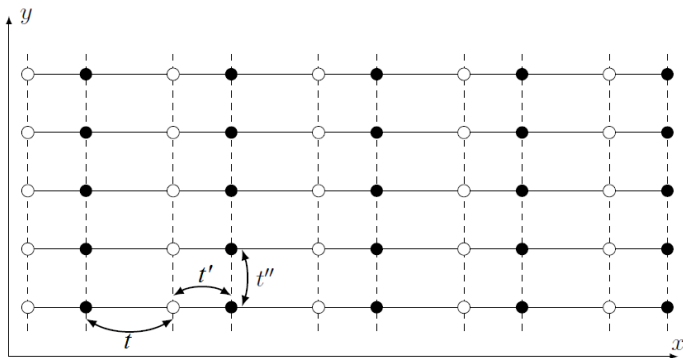


FIG. 7. Chains of dimers coupled in the  $y$  direction by a hopping parameter  $t''$ .

bulk Hamiltonian of the coupled chains reads

$$\mathcal{H}_{cc}^B = -t'' \cos(k_y b_0) \mathbb{1} + \mathcal{H}^B, \quad (26)$$

with  $b_0$  the distance between two chains. We see that the term proportional to  $\mathbb{1}$  involves a dispersion along the  $y$  direction and does not change the properties of the Zak phase which are encoded in  $\mathcal{H}^B$ . Therefore, two distinct topological phases ( $\mathcal{Z} = 0$  and  $\mathcal{Z} = \pi$ ) arise when the criteria given in Eq. (16) is satisfied. This means that when  $\mathcal{Z} = \pi$ , a ribbon of finite width in the  $x$  direction and invariant by translation in the  $y$  direction supports dispersive edge states along its edges, as shown in Fig 8.

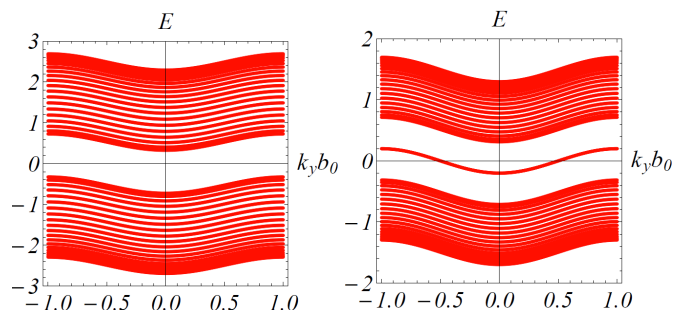


FIG. 8. Energy levels of a ribbon built from chains of  $M = 20$  dimers. The chains are coupled one to each other in the  $y$  direction with a hopping parameter  $t'' = 0.1$ , and the ribbon is invariant by translation along this direction. We took  $t = 1$ , and (left)  $t' = 1.5$ , (right)  $t' = 0.5$ . In the first case the Zak phase is  $\mathcal{Z} = 0$  and there is no edge state. In the other case, the Zak phase is  $\mathcal{Z} = \pi$  and dispersive edge states have emerged in the gap.

This example shows that the Zak phase may help characterizing the edge states even in the absence of a chiral symmetry. In addition, it also illustrates that the Zak phase, which until now we have defined for a one-dimensional system, may provide informations about the edge states in systems of higher dimension. In the following of the paper, we investigate the more complex case of a monolayer of graphene.

### III. THE ZAK PHASE AND THE EDGE STATES OF GRAPHENE RIBBONS

Turning now to graphene, we demonstrate in this section that the Zak phase, introduced in section II for a one-dimensional system, has a natural generalization for a large class of two-dimensional graphene ribbons. In the particular case of zigzag edges, following the same lines as in the 1D case, we prove that it is possible to relate the Zak phase to the existence of edge states. We then consider the case of ribbons with arbitrary orientations, and show that, computing the Zak phase, we can predict the presence or absence of edge states according to the nature of the edge.

#### A. The bulk Hamiltonian

We describe the electronic spectrum of graphene by a tight-binding model on the triangular Bravais lattice with two atoms ( $A$  and  $B$ ) per unit cell, as illustrated in Fig. 9. The parameters  $t_1$ ,  $t_2$  and  $t_3$  represent the three hopping integrals between nearest neighbors and for now we consider the isotropic case  $t_1 = t_2 = t_3$  (the anisotropic case is treated in Sec. IV). The vectors  $\mathbf{a}_1$  and  $\mathbf{a}_2$  form a basis of the Bravais lattice, and we note  $(\mathbf{a}_1^*, \mathbf{a}_2^*)$  (with  $\mathbf{a}_i^* \cdot \mathbf{a}_j = 2\pi\delta_{ij}$ ) the associated basis of the reciprocal space. For periodic bound-

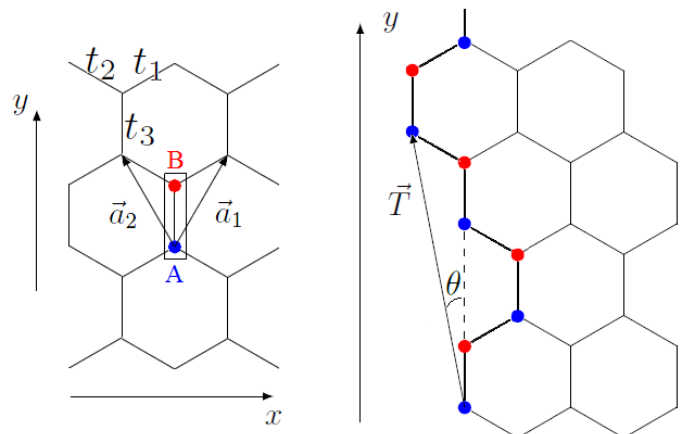


FIG. 9. (Left) Unit cell (dimer)  $A$ - $B$  of the graphene sheet with the basis vectors of the Bravais lattice  $\mathbf{a}_1$  and  $\mathbf{a}_2$  and the hopping parameters  $t_1$ ,  $t_2$  and  $t_3$ . (Right) Example of an edge obtained by translating the dimer along  $\mathbf{a}_1$ , then twice along  $\mathbf{a}_2$ . This edge is characterized by the periodicity vector  $\mathbf{T} = \mathbf{a}_1 + 2\mathbf{a}_2$ .

ary conditions in both  $x$  and  $y$  directions, Bloch theorem leads to the bulk Hamiltonian

$$H^B(\mathbf{k}) = -t_3 |\rho(\mathbf{k})| \begin{pmatrix} 0 & e^{-i\phi(\mathbf{k})} \\ e^{i\phi(\mathbf{k})} & 0 \end{pmatrix} \quad (27)$$

in the basis of the two sub-lattices  $A$  and  $B$ , with

$$\begin{aligned} \rho(\mathbf{k}) &= 1 + \frac{t_1}{t_3} \exp(-i\mathbf{k} \cdot \mathbf{a}_1) + \frac{t_2}{t_3} \exp(-i\mathbf{k} \cdot \mathbf{a}_2) \\ &= |\rho(\mathbf{k})| e^{-i\phi(\mathbf{k})}. \end{aligned} \quad (28)$$

The eigenenergies of the bulk Hamiltonian  $H^B(\mathbf{k})$  consist in two bands, given by  $\epsilon_{\pm}(\mathbf{k}) = \pm t_3 |\rho(\mathbf{k})|$ , and the corresponding eigenvectors have the form,

$$|u_{\mathbf{k},\pm}\rangle = \frac{1}{\sqrt{2}} \begin{pmatrix} e^{-i\phi(\mathbf{k})} \\ \pm 1 \end{pmatrix}. \quad (29)$$

The positive and negative bands touch linearly at two inequivalent points  $\mathbf{D}$  and  $\mathbf{D}'$  (the Dirac points) which, in the isotropic case considered in this section, are located at the corners  $\mathbf{K}$  and  $\mathbf{K}'$  of the first Brillouin zone.

The Hamiltonian (27) can be written in the same form  $H^B(\mathbf{k}) = -t_3 \mathbf{g}(\mathbf{k}) \cdot \sigma$  as for the chain of dimers (5), the difference being that  $\mathbf{k}$  is now a two-dimensional vector and that the  $\mathbf{k}$  dependence of  $\mathbf{g}(\mathbf{k})$  is of course different. As in our 1D toy model, topological properties of the wave function as well as some characterization of the edge states are expected to be encoded in the loops drawn by  $\mathbf{g}(\mathbf{k})$  as  $\mathbf{k}$  varies across the Brillouin zone. This connection was actually already suggested by Ryu and Hatsugai<sup>14</sup> in the broader context of systems with chiral symmetry (and more recently by Mong and Shivamoggi in a general study of Dirac Hamiltonians<sup>15</sup>). Their approach, which basically consists in the graphical evaluation of the Zak phase in the same way as in Fig. 3, was applied for three different regular types of edges (zigzag, armchair and bearded edges). Comparing with numerical calculations, they showed that the Zak phase could correctly predict the existence of edge states in these cases. However, their approach relied on the construction of a *specific* bulk Hamiltonian (i.e. a vector  $\mathbf{g}(\mathbf{k})$ ) for each type of edge considered, and is therefore not convenient to consider arbitrary boundary conditions. Here, we keep the *same* bulk Hamiltonian but we associate to each type of edge a *specific* 2D Brillouin zone. This allows us to predict the existence of edge states for different ribbon geometries, and therefore to address a significantly larger class of ribbons.

## B. Edges of graphene ribbons

Turning now to graphene ribbons, we assume that both edges of the ribbon are parallel (i.e. that one edge can be deduced from the other by translation of a lattice vector  $\mathbf{C}$ ) and constructed as illustrated in Fig. 9, i.e. by connecting dimers  $A$ - $B$  (or unit cells) of *fixed orientation* (vertical orientation in Fig. 9).

More precisely, considering two positive or negative integers  $m$  and  $n$ , an edge is built as  $(|m| + |n|)$  translations of the dimer,  $|m|$  of which along  $\mathbf{a}_1$  ( $-\mathbf{a}_1$  if  $m$  negative) and  $|n|$  of which along  $\mathbf{a}_2$  ( $-\mathbf{a}_2$  if  $n$  negative), in an arbitrary order, and by repeating the pattern obtained in this way. Therefore the edges are invariant under the translation vector  $\mathbf{T} = m\mathbf{a}_1 + n\mathbf{a}_2$  which characterizes the type of edge. Noting  $\theta$  the angle between  $\mathbf{T}$  and the  $y$  axis, this angle is related to  $(m, n)$  through

$$\tan \theta = \frac{1}{\sqrt{3}} \frac{n - m}{n + m}. \quad (30)$$

When  $m$  and  $n$  have the same sign, the class of edges constructed in this way exactly corresponds to the minimal boundary conditions of Akhmerov and Beenakker.<sup>23</sup> In the other case, the edges exhibit dangling bonds.

Fig. 1 gives some examples of such edges. It is easy to see that the vectors  $\mathbf{T}(m, n)$  and  $\mathbf{T}(n, m)$  describe the same kind of edge. We also notice that the same vector  $\mathbf{T}$  can describe edges with different shapes, see the example of  $\mathbf{T} = (2, 5)$  in Fig. 1.

We stress that choosing the “unit-cell” dimer  $A$ - $B$  with a different orientation (i.e. rotated from  $\pm 2\pi/3$  with respect to the vertical one used in Fig. 9) leads to a different set of boundaries. These latter are of course just deduced from the former by a  $\pm 2\pi/3$  rotation, and thus considering only the vertical unit-cell dimer, as we shall do in the following, does not restrict the type of edge to be studied. We insist however that if one wanted to consider another orientation of the unit-cell dimer for the edges, it would be essential to *modify accordingly the dimer orientation* in the definition of the *bulk* Hamiltonian (which basically fixes the zero of the phase  $\phi(\mathbf{k})$  in Eqs. (27) or (29)). This is a necessary condition to derive a bulk-edge correspondence for the edge states in terms of the Zak phase.

## C. The Zak phase in graphene ribbons

For one-dimensional models such as the one considered in section II, the Zak phase is defined as the integral of the Berry connection across the Brillouin zone. To generalize this notion to two-dimensional systems such as graphene, this integration should be taken on a cut of a 2D Brillouin zone in a direction transverse to the ribbon orientation. More precisely, as the ribbon is assumed to be invariant under translation by the vector  $\mathbf{T}$ , Bloch theorem guarantees that  $k_{\parallel}$ , the component of the crystal momentum parallel to  $\mathbf{T}$ , is a good quantum number. We expect therefore the Zak phase  $\mathcal{Z}(k_{\parallel})$  to be a function of  $k_{\parallel}$ , and to correspond to an integration of the Berry connection across the 2D Brillouin zone along a perpendicular direction  $k_{\perp}$ .

Let us assume for now that  $m$  and  $n$  are coprime integers (we will return below to the case where they are not). We choose the Brillouin zone from which the Zak phase will be computed as the one generated by two orthogonal vectors of the reciprocal space,  $\Gamma_{\parallel}$  and  $\Gamma_{\perp}$ , obtained as follows. The first of these vector  $\Gamma_{\parallel} \equiv 2\pi\mathbf{T}/|\mathbf{T}|^2$  is parallel to the direction  $\mathbf{T}$  of the ribbon and merely defines the one-dimensional Brillouin zone of the ribbon. The second vector  $\Gamma_{\perp}$  is taken perpendicular to  $\mathbf{T}$ , and its norm is fixed by the constraint that  $\Gamma_{\parallel} \times \Gamma_{\perp} = \mathbf{a}_1^* \times \mathbf{a}_2^*$  (where, as mentioned above,  $\mathbf{a}_1^*$  and  $\mathbf{a}_2^*$  are the reciprocal lattice vectors defined by  $\mathbf{a}_i \cdot \mathbf{a}_j^* = 2\pi\delta_{ij}$ ). This leads to

$$\Gamma_{\parallel}(m, n) = \frac{(n + 2m)\mathbf{a}_1^* + (m + 2n)\mathbf{a}_2^*}{2(n^2 + m^2 + nm)} \quad (31)$$

$$\Gamma_{\perp}(m, n) = n\mathbf{a}_1^* - m\mathbf{a}_2^*. \quad (32)$$

For the sake of completeness we remind briefly in appendix A why  $(\Gamma_{\parallel}, \Gamma_{\perp})$  constructed in this way actually defines a Brillouin zone when  $(m, n)$  are coprime integers, and only in this case.

For an arbitrary edge characterized by the vector  $\mathbf{T}(m, n)$ , we introduce the unit vectors  $\mathbf{e}_{\parallel} = \Gamma_{\parallel}/|\Gamma_{\parallel}|$  and  $\mathbf{e}_{\perp} =$

$\Gamma_{\perp}/|\Gamma_{\perp}|$ , and write the momentum as  $\mathbf{k} = k_{\parallel}\mathbf{e}_{\parallel} + k_{\perp}\mathbf{e}_{\perp}$ . The Zak phase  $\mathcal{Z}(k_{\parallel})$  can thus be defined as:

$$\mathcal{Z}(k_{\parallel}) = i \oint dk_{\perp} \langle u_{\mathbf{k},\pm} | \partial_{k_{\perp}} u_{\mathbf{k},\pm} \rangle, \quad (33)$$

which, by using the expression of the Bloch function (29), simply reads

$$\mathcal{Z}(k_{\parallel}) = \frac{1}{2} \oint dk_{\perp} \partial_{k_{\perp}} \phi(\mathbf{k}). \quad (34)$$

Note that as  $\Gamma_{\perp}$  is a vector of the reciprocal lattice, the integration can indeed be seen as taken on a closed path.

Let us consider now the situation where  $m$  and  $n$  are not coprime, in which case  $(\Gamma_{\parallel}, \Gamma_{\perp})$  obtained from Eqs. (31) and (32) do not form a basis of the reciprocal lattice (see appendix A). Writing  $m = l\tilde{m}$  and  $n = l\tilde{n}$  with  $l$  integer and  $\tilde{m}$  and  $\tilde{n}$  coprime and following exactly the same line of argument as above, we can construct a basis  $(\tilde{\Gamma}_{\parallel}, \tilde{\Gamma}_{\perp})$  of the reciprocal lattice corresponding to  $(\tilde{m}, \tilde{n})$ , and define the Zak phase  $\mathcal{Z}_{(\tilde{m}, \tilde{n})}(\tilde{k}_{\parallel})$  accordingly from (34). An example of such a construction will be shown in Sec. III E (see the case  $(m, n) = (2, 0)$  of Fig. 13). However, as  $\mathbf{T}(\tilde{m}, \tilde{n}) = \mathbf{T}(m, n)/l$ , we have now  $\tilde{\Gamma}_{\parallel} = l\Gamma_{\parallel}$ . As a consequence, to a given value  $k_{\parallel}$  of the quantum number of the ribbon correspond  $l$  values  $(\tilde{k}_{\parallel}^{(0)}, \dots, \tilde{k}_{\parallel}^{(l-1)})$  in the Brillouin zone ( $\tilde{k}_{\parallel}^{(j)} = k_{\parallel} + j|\tilde{\Gamma}_{\parallel}|$ ), and therefore  $l$  Zak phases. The prescription we shall use for non-coprime integers  $(m, n)$  is therefore that for a given value  $k_{\parallel}$  of the ribbon quantum number, the Zak phase is defined as

$$\mathcal{Z}_{(m,n)}(k_{\parallel}) \equiv \sum_{j=1}^l \mathcal{Z}_{(\tilde{m}, \tilde{n})}(\tilde{k}_{\parallel}^{(j)}). \quad (35)$$

This prescription merely corresponds to a folding of the Brillouin zone.

#### D. Zigzag boundary conditions

Before we address general orientations for the graphene ribbon, let us first consider in details the simple case of zigzag boundary conditions. In that case, and as illustrated in Fig. 10, the two edges of the ribbon, ( $\mathcal{B}_1$ ) and ( $\mathcal{B}_2$ ), are constructed as the vertical dimer  $A$ - $B$  translated periodically with the vector  $\mathbf{T} = \mathbf{a}_1$  (see Fig. 9). We note  $\mathbf{C}$  the vector which connects the two edges and  $\mathbf{C}' = \mathbf{C} + 2\mathbf{a}_2 - \mathbf{a}_1$  the vector connecting  $\mathcal{B}'_1$  and  $\mathcal{B}'_2$ , the lines of empty sites nearest neighbors to the edges  $\mathcal{B}_1$  and  $\mathcal{B}_2$ . Noting  $\Psi_{\mathbf{k}\pm} = (\Psi_{\mathbf{k}\pm}^A, \Psi_{\mathbf{k}\pm}^B)^T$  the Bloch state of momentum  $\mathbf{k}$ , we have

$$\Psi_{\mathbf{k},\pm}(\mathbf{r}) = \langle \mathbf{r} | \Psi_{\mathbf{k}\pm} \rangle \propto \frac{e^{i\mathbf{k}\cdot\mathbf{r}}}{\sqrt{2}} \begin{pmatrix} e^{-i\phi(\mathbf{k})} \\ \pm 1 \end{pmatrix}. \quad (36)$$

Following the approach used for the one-dimensional chain of dimers of section II B, we would like to construct eigenstates of the ribbon as a linear combination  $\Psi$  of two Bloch states  $\Psi_{\mathbf{k}\pm}$  and  $\Psi_{\mathbf{k}'\pm}$  at the same energy. From Fig. 10, we see that the boundary conditions read

$$\Psi^A(\mathbf{C}' + \nu\mathbf{T}) = 0 \quad [\text{on } \mathcal{B}'_2], \quad (37)$$

$$\Psi^B(\nu\mathbf{T}) = 0 \quad [\text{on } \mathcal{B}'_1], \quad (38)$$

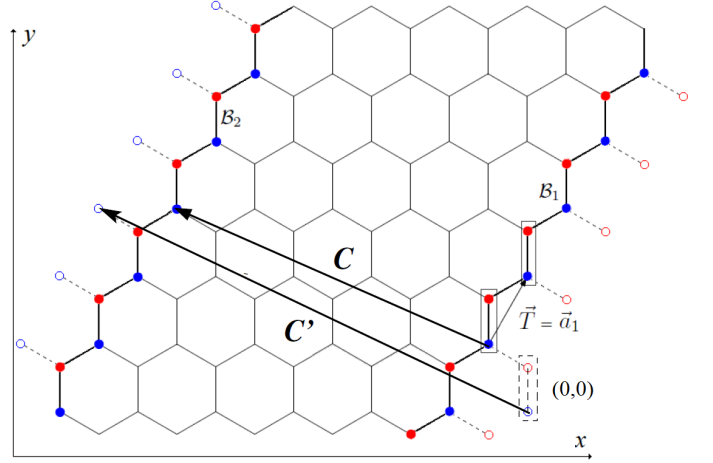


FIG. 10. Schematic representation of a zigzag ribbon. The zigzag edge is obtained by translating the dimer  $A$ - $B$  (represented by a rectangle) with the periodicity  $\mathbf{T} = \mathbf{a}_1$ . The two edges  $\mathcal{B}_1$  and  $\mathcal{B}_2$  are represented by thick lines. The first vacant sites outside of the ribbon where we impose the wave function to vanish are represented by circles.  $\mathbf{C}$  is the vector of the Bravais lattice which connects two sites on both edges, and  $\mathbf{C}'$  connects the first vacant site on one side of the ribbon to the first vacant site on the other side.

with  $\nu \in \mathbb{Z}$ .

The boundary condition Eq. (38) implies that the wave functions  $\Psi$  are combinations of the form  $\Psi = \Psi_{\mathbf{k}} - \Psi_{\mathbf{k}'}$  with  $\mathbf{k} \cdot \mathbf{T} = \mathbf{k}' \cdot \mathbf{T}$  (here  $\mathbf{T} = \mathbf{a}_1$ ). Since we need  $\epsilon_{\mathbf{k}} = \epsilon_{\mathbf{k}'}$ , we have to consider momentum pairs  $(\mathbf{k}, \mathbf{k}')$  such that  $(\mathbf{k} + \mathbf{k}') \cdot \mathbf{a}_2 = \mathbf{k} \cdot \mathbf{a}_1 = \mathbf{k}' \cdot \mathbf{a}_1$ . For a given value of  $k_{\parallel}$ , it can be checked that this is satisfied if

$$\mathbf{k} = \mathbf{k}_{\parallel} + \mathbf{k}_{\perp}, \quad (39)$$

$$\mathbf{k}' = \mathbf{k}_{\parallel} - \mathbf{k}_{\perp}, \quad (40)$$

where we have introduced  $\mathbf{k}_{\parallel} = k_{\parallel}\mathbf{e}_{\parallel}$  and  $\mathbf{k}_{\perp} = k_{\perp}\mathbf{e}_{\perp}$ . Note that  $\mathbf{k}_{\perp} = 0$  or  $\mathbf{k}_{\perp} = \Gamma_{\perp}/2$  correspond to  $\Psi_{\mathbf{k}} - \Psi_{\mathbf{k}'} \equiv 0$ .

The boundary condition Eq. (38) then imposes

$$(\mathbf{k} - \mathbf{k}') \cdot \mathbf{C}' - (\phi(\mathbf{k}) - \phi(\mathbf{k}')) = 2\kappa\pi \quad (41)$$

(for integer  $\kappa$ ), or in term of the phase  $\phi(k_{\parallel}, k_{\perp}) = \frac{1}{2}[\phi(\mathbf{k}_{\parallel} + \mathbf{k}_{\perp}) - \phi(\mathbf{k}_{\parallel} - \mathbf{k}_{\perp})]$

$$\mathbf{k}_{\perp} \cdot \mathbf{C}' - \phi(k_{\parallel}, k_{\perp}) = \kappa\pi, \quad (42)$$

which is the strict equivalent of the quantization condition (14) obtained for the 1D chain. We note furthermore that  $(\Gamma_{\perp} \cdot \mathbf{C}') = 2\pi(M + 1)$ , with  $M$  the number of dimers in the transverse direction of the ribbon, and thus half the number of bands. Using the same arguments as in section II B, we see that the number of edge states depends on the value of  $\phi(k_{\parallel}, \Gamma_{\perp}/2)$ , and more precisely that the quantity

$$\left| \frac{\mathcal{Z}(k_{\parallel})}{\pi} \right| = \left| \frac{1}{2\pi} \oint dk_{\perp} \frac{d\phi(k_{\parallel}, k_{\perp})}{dk_{\perp}} \right| \quad (43)$$

gives the number of pairs of edge states (with opposite energies) for a given  $k_{\parallel}$ .

#### E. General orientation

We consider now graphene ribbons characterized by an arbitrary translation vector  $\mathbf{T}(m, n)$ . Based on similar argu-

ments as in the previous section we conjecture that the relation between the Zak phase and the number of edge states holds in this general case. Then we use this relation to predict the existence of edge states in graphene ribbons of general orientation. We also check that for every case for which edge states has been computed (numerically or otherwise) their appearance is correctly predicted by the Zak phase.

In Eq. (34), the phase  $\phi(\mathbf{k})$  should be understood as a multivalued function. The single-valued function  $\tilde{\phi}(\mathbf{k})$  corresponding to the restriction of  $\phi(\mathbf{k})$  to the interval  $[-\pi, +\pi]$  is displayed on Fig. 11. It shows lines of discontinuity connecting pairs of Dirac points. The location of the discontinuities (i.e. which Dirac points are connected by them) depends on the choice made for the unit cell dimer  $A$ - $B$  (oriented along the  $y$  axis in this paper, see Fig. 9). Therefore the phase  $\phi(\mathbf{k})$  is not invariant by a rotation of an angle  $\pm 2\pi/3$ .

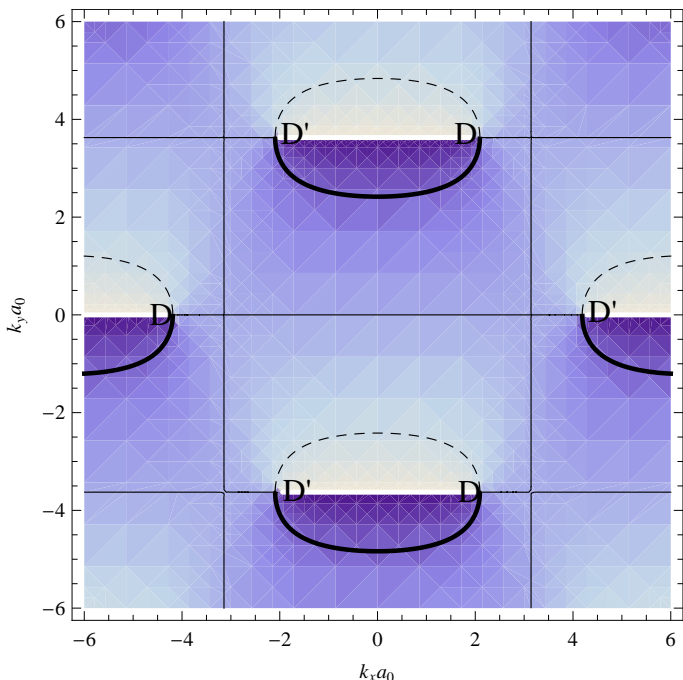


FIG. 11. Density plot of the phase  $\tilde{\phi}(\mathbf{k})$ . The discontinuities of the phase are shown by horizontal white lines connecting pairs of Dirac points. These singularities separate the values  $\phi = +\pi$  (light region) to the value  $\phi = -\pi$  (dark region). Consequently, the only paths  $\Gamma_{\perp}$  that contribute to a non-vanishing Zak phase are those that cross these singularities. The black lines, thick lines and dashed lines represent the iso- $\tilde{\phi}$  lines respectively for  $\tilde{\phi} = 0$ ,  $\tilde{\phi} = -\pi/2$  and  $+\pi/2$ .

Let us start again by considering ribbons of period  $\mathbf{T}(m, n)$  with coprime  $(m, n)$ . The discontinuities of  $\tilde{\phi}(\mathbf{k})$  are extremely convenient to determine the Zak phase since paths that lead to a non-vanishing Zak phase necessarily cross a discontinuity line. Actually, the Zak phase  $\mathcal{Z}_{(m,n)}(k_{\parallel})$  is given by the number of discontinuities  $d(k_{\parallel})$  intersected by the path  $\mathcal{P}_{(m,n)}(k_{\parallel}) = [\mathbf{k}_{\parallel}, \mathbf{k}_{\parallel} + \mathbf{\Gamma}_{\perp}]$  along which  $\mathcal{Z}_{(m,n)}(k_{\parallel})$  is computed, that is

$$\mathcal{Z}(k_{\parallel}) = \pm\pi d(k_{\parallel}). \quad (44)$$

In other words,  $d(k_{\parallel})$  is just the number of pairs of edge states (of opposite energies) for a given  $k_{\parallel}$ .

These considerations make it possible to compute graphically the Zak phase in a rather straightforward way. For a

given choice of edge characterized by the vector  $\mathbf{T}(m, n) = m\mathbf{a}_1 + n\mathbf{a}_2$ , we first represent the vector  $\mathbf{\Gamma}_{\perp}(m, n) = n\mathbf{a}_1^* - m\mathbf{a}_2^*$  (Eq. 32). This is done in Fig. 12, where we plot the vectors  $\mathbf{\Gamma}_{\perp}(m, n)$  from the left extremity of the discontinuity  $(0, 0)$  to the left extremity of the discontinuity  $(n, -m)$ . Next, in Fig. 13, we translate perpendicularly  $\mathbf{\Gamma}_{\perp}$  until the left extremity of another discontinuity is reached (dashed line), which gives  $\mathbf{\Gamma}_{\parallel}(m, n)$ . The rectangle defined by  $\mathbf{\Gamma}_{\perp}$  and  $\mathbf{\Gamma}_{\parallel}$  is the Brillouin zone we want to associate with the ribbon. For a given value of the momentum  $k_{\parallel}$ ,  $\mathcal{Z}(k_{\parallel})$  is then deduced from Eq. (44) by simply counting the number of intersections of the segment  $[\mathbf{k}_{\parallel}, \mathbf{k}_{\parallel} + \mathbf{\Gamma}_{\perp}]$  with the discontinuity lines of  $\tilde{\phi}(\mathbf{k})$ .

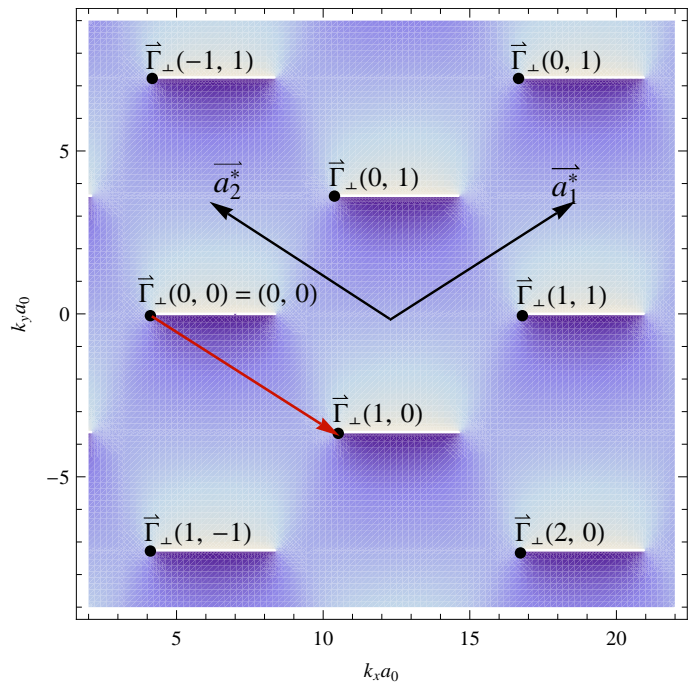


FIG. 12. On top of the density plot of the phase  $\tilde{\phi}(\mathbf{k})$ , we have represented several values of the vector  $\mathbf{\Gamma}_{\perp}(m, n) = n\mathbf{a}_1^* - m\mathbf{a}_2^*$ . The left extremity of a discontinuity of  $\tilde{\phi}(\mathbf{k})$  is taken as the origin. We have explicitly plotted the vector  $\mathbf{\Gamma}_{\perp}(1, 0)$  as an example.

If  $m$  and  $n$  are not coprime, as for instance in Fig. 13(d),  $\mathbf{\Gamma}_{\parallel}(m, n)$  and  $\mathbf{\Gamma}_{\perp}(m, n)$  cannot be obtained in this way as they do not define a Brillouin zone. Writing however  $(m, n) = l(\tilde{m}, \tilde{n})$  with  $(\tilde{m}, \tilde{n})$  coprime, the Brillouin zone corresponding to  $(\tilde{m}, \tilde{n})$  can be constructed as above, and one has simply  $\mathbf{\Gamma}_{\parallel}(m, n) = \tilde{\mathbf{\Gamma}}_{\parallel}(\tilde{m}, \tilde{n})/l$  and  $\mathbf{\Gamma}_{\perp}(m, n) = l\tilde{\mathbf{\Gamma}}_{\perp}(\tilde{m}, \tilde{n})$ , which basically amounts to a folding of  $\tilde{\mathbf{\Gamma}}_{\parallel}$  by a factor  $l$ . For a given value of  $k_{\parallel}$ , the Zak phase is then given by Eq. (35).

### F. Range of existence and density of edge states

In this section we derive the range  $\Delta k_{\parallel}$  for which edge states exist, as well as the density of edge states for arbitrary boundary conditions thanks to the bulk-edge correspondence in terms of the Zak phase.

In the last section, we showed that the number of pairs of edge states for a given value of  $k_{\parallel}$  is given by the number  $d(k_{\parallel})$  of crossings between the path  $\mathcal{P}_{(m,n)}(k_{\parallel})$  and the discontinuities of  $\tilde{\phi}(\mathbf{k})$ . Since a Brillouin zone always contains



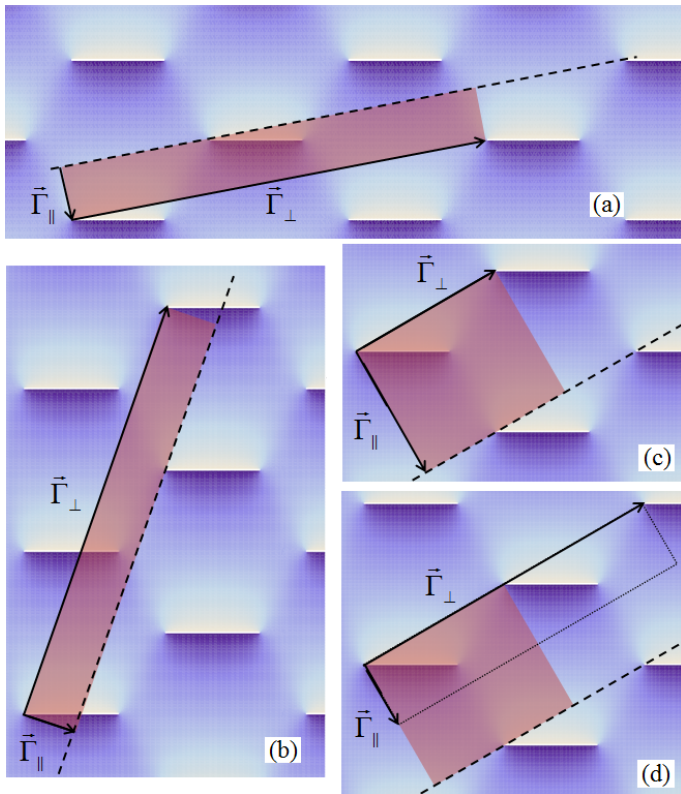


FIG. 13. Surfaces  $|\Gamma_{\parallel} \wedge \Gamma_{\perp}|$  associated with different ribbon vectors  $\mathbf{T}(m, n)$ .  $\Gamma_{\perp}$  is obtained as  $\Gamma_{\perp}(m, n) = na_1^* - ma_2^* = (n, -m)$ ; see text for the construction of  $\Gamma_{\parallel}$ . (a)  $\Gamma_{\perp}(m = 1, n = 2) = (2, -1)$ , (b)  $\Gamma_{\perp}(-2, 3) = (3, 2)$ , and (c)  $\Gamma_{\perp}(0, 1) = (1, 0)$ . In these three cases,  $m$  and  $n$  are coprime, and the surfaces  $|\Gamma_{\parallel} \wedge \Gamma_{\perp}|$  represented by a shaded rectangles are Brillouin zones. (d)  $\mathbf{T}(0, 2)$ : the surface obtained by  $\Gamma_{\parallel}$  and  $\Gamma_{\perp}$  is not a Brillouin zone because  $m$  and  $n$  are not coprime. The corresponding Brillouin zone (shaded rectangle) is given by  $\Gamma_{\perp}(0, 1) = \Gamma_{\perp}(0, 2)/2$  and  $\Gamma_{\parallel}(1, 0) = 2\Gamma_{\parallel}(2, 0)$ .

exactly one line of discontinuities, the total range

$$\Delta k_{\parallel} \equiv \int_0^{2\pi/|\mathbf{T}|} d(k_{\parallel}) dk_{\parallel} \quad (45)$$

over which the ribbon exhibits edge states, is obtained by projecting the line of discontinuities onto the  $k_{\parallel}$  axis, as illustrated in Fig. 14. This leads to

$$\Delta k_{\parallel} = \frac{4\pi}{3a_0} |\sin \theta|, \quad (46)$$

where  $\theta$  is the angle between the direction  $\mathbf{T}$  of the ribbon and the vertical axis  $y$  of the dimers (see Fig. 9 and Eq. (30)). Therefore, there is no edge state for edges parallel to the armchair edge ( $\theta = 0$ ) and  $\Delta k_{\parallel}$  is maximum and equal to  $4\pi/3a_0$  for bearded edges.<sup>18,19</sup> Then, from Eq. (30) we have the relation between the range  $\Delta k_{\parallel}$  of existence of edge states in graphene and the integers  $(m, n)$  characterizing the edge:

$$\Delta k_{\parallel}(m, n) = \frac{2\pi}{3a_0} \frac{|n - m|}{\sqrt{n^2 + m^2 + nm}}. \quad (47)$$

We notice that  $\Delta k_{\parallel}(m, n) = \Delta k_{\parallel}(lm, ln)$  which means that  $\mathbf{T}(m, n)$  and  $l\mathbf{T}(m, n)$  support the same number of localized states. A relevant quantity to study is the ratio  $\mathcal{R} \equiv$

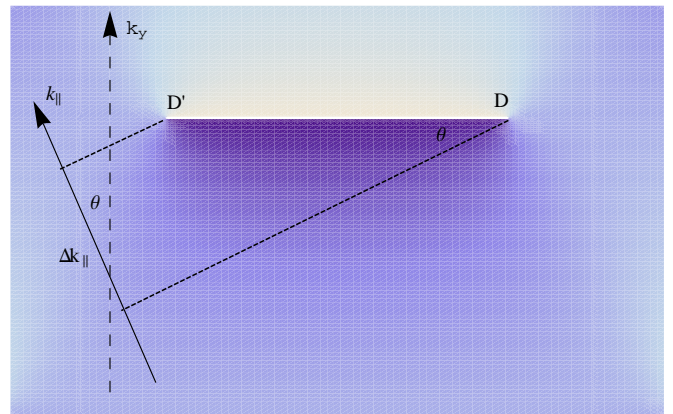


FIG. 14. Projection of the discontinuity of  $\tilde{\phi}(\mathbf{k})$  onto the  $k_{\parallel}$  axis. This projection gives the range  $\Delta k_{\parallel}$  for the existence of edge states.

$\Delta k_{\parallel}/|\Gamma_{\parallel}| = \Delta k_{\parallel}|\mathbf{T}|/(2\pi)$  which gives the relative range of the 1D Brillouin zone where edge states exist. We find

$$\mathcal{R} = \frac{|n - m|}{3}. \quad (48)$$

We now comment the formulas (47) and (48). First, we apply these formulas to several types of edges listed in table I. The three general types of edges mentioned in this table

	$(m, n)$	$\Delta k_{\parallel}$	$\mathcal{R}$
armchair	(1, 1)	0	0
zigzag	(1, 0)	$2\pi/3a_0$	1/3
bearded zigzag	(1, -1)	$4\pi/3a_0$	2/3
bearded armchair	(2, -1)	$2\pi/\sqrt{3}a_0$	1
general types	(1, 3)	$4\pi/3\sqrt{13}a_0$	2/3
	(1, 5)	$2\pi/3\sqrt{31}a_0$	4/3
	(1, 8)	$14\pi/15\sqrt{3}a_0$	7/3

TABLE I. Applications of the formulas (47) and (48) for some edge geometries studied in previous works.

represent a zigzag profile extending over respectively three, five and eight unit cells followed by an armchair defect (see for example Fig. 1 for the case (1, 5)). These results are in good agreement with the size of the edge states energy bands obtained by numerical tight-binding calculations in different previous works.<sup>2,3,14,20-22</sup> We also notice that in the limit  $|n| \gg |m|$  (or the other way), we recover  $\Delta k_{\parallel} \rightarrow 2\pi/3a_0$  which is the expected result for the zigzag edge.

The formulas (47) and (48) directly lead to the important result that edge states exist for most types of ribbons with a periodic pattern, which is in agreement with a previous analytical approach within the Dirac framework.<sup>23</sup> More precisely, we find that there is no edge state if and only if  $n = m$ . As already mentioned, this class of ribbons includes all the vectors  $\mathbf{T}$  parallel to the  $y$  axis of the dimers  $A - B$  (see for instance the case (3, 3) displayed in Fig. 1. Similar ribbons have been synthesized for the first time recently<sup>28</sup>). The well-known particular armchair case corresponds to the smallest  $|\mathbf{T}|$  that obeys this condition.

The case  $\mathcal{R} \geq 1$  also deserves some attention. It implies that two or more pairs of localized states may correspond to the same  $k_{\parallel}$ . This situation happens when, as

illustrated in the example of Fig. 13(b), several discontinuities are intersected by the path  $\mathcal{P}_{(m,n)}(k_{\parallel})$ . Such a situation is automatically achieved for  $m$  and  $n$  coprime when  $\theta(m,n) > \theta(4,1) = \arctan(\sqrt{3}/5)$ . Moreover, by construction, the projection of the line of discontinuity of  $\tilde{\phi}$  spans  $\mathcal{R}$  times the Brillouin zone, which implies that the number of localized states cannot differ by more than one unit for any two  $k_{\parallel}$  (see Fig. 15). Therefore, for  $m$  and  $n$  coprime, there

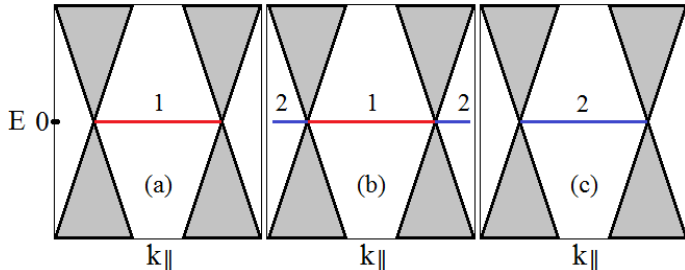


FIG. 15. Schematic band structures of graphene ribbons that exhibit edge states. Edge states are represented as zero-energy flat bands as expected in the large width limit within the tight-binding model (assuming the chiral symmetry is preserved). The number of pairs of edge-states is indicated on the figure. (a) corresponds to the case  $\mathcal{R} < 1$ , (b) corresponds to  $\mathcal{R} > 1$ . (c) Our analysis based on the Zak phase predicts that this configuration is not allowed.

is either  $[\mathcal{R}]$  or  $[\mathcal{R}] + 1$  edge states for each  $k_{\parallel}$  ( $[x]$  is the floor function). In the particular case where  $\mathcal{R}$  is an integer there are exactly  $\mathcal{R}$  edge states for each  $k_{\parallel}$ .

Finally, we can define the quantity  $\rho = \mathcal{R}/|\mathbf{T}|$  which corresponds to the “density of edge states per unit length” introduced by Akhmerov and Beenakker. We get

$$\rho = \frac{\Delta k_{\parallel}}{2\pi} = \frac{1}{3a_0} \frac{|n-m|}{\sqrt{n^2+m^2+nm}}, \quad (49)$$

which was first obtained in Ref. [23] for minimal boundary conditions by a different method.

#### IV. EMERGENCE AND DESTRUCTION OF EDGE STATES: A TOPOLOGICAL APPROACH

In this section, we generalize the formula (47) for non-equal hopping parameters  $t_1 \neq t_2 \neq t_3$ , and establish a criterion for the existence of edge states for an anisotropic honeycomb lattice. We show that the manipulation of these parameters leads to a topological transition described in terms of Zak phase that affects the range  $\Delta k_{\parallel}$  of existence of edge states. We stress that breaking the isotropy of the hopping parameters preserves the chiral symmetry, and therefore the topological character of the Zak phase. As a consequence the analysis developed in the previous section generalizes straightforwardly to the case considered below.

##### A. Effect of an anisotropy on the existence of edge states

Several previous works dealing with the tight-binding model in the honeycomb lattice showed that the Dirac points move when modifying the ratio of the parameters  $t_i/t_j$ .<sup>29–32</sup>

As the lines of discontinuities of  $\tilde{\phi}(\mathbf{k})$  connect pairs of Dirac points, the modification of the ratio  $t_i/t_j$  changes the Zak phase and therefore leads to new ranges  $\Delta k_{\parallel}$  of existence of edge states. This is clearly shown in Fig. 16. To determine

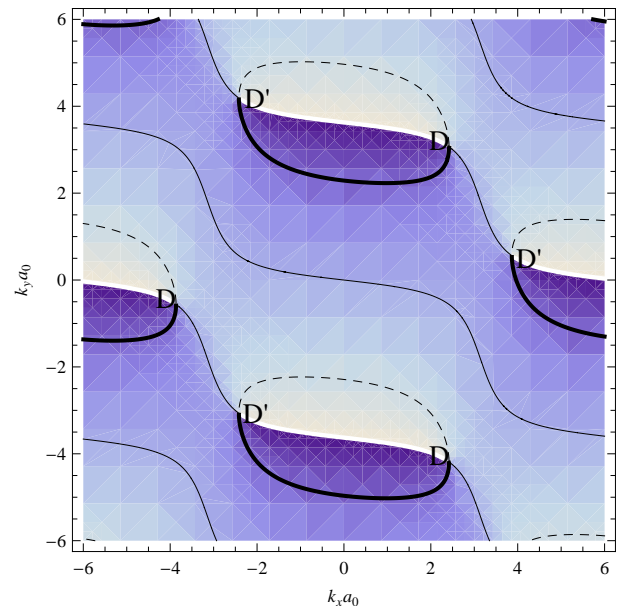


FIG. 16. Density plot of the phase  $\tilde{\phi}(\mathbf{k})$  for  $t_2 = 1.5t_1 = 1.5t_3$ . The discontinuities of the phase are shown by curved white lines that pair the Dirac points. The black lines, thick lines and dashed lines represent the iso- $\tilde{\phi}$  lines respectively for  $\tilde{\phi} = 0$ ,  $\tilde{\phi} = -\pi/2$  and  $+\pi/2$ .

these new ranges, we have first to specify the position of the Dirac points for any  $t_i$ . Up to a vector of the reciprocal lattice, they are given by

$$\begin{aligned} \mathbf{D} &= -\frac{\pi-d_1}{2\pi} \mathbf{a}_1^* + \frac{\pi-d_2}{2\pi} \mathbf{a}_2^* \\ \mathbf{D}' &= \frac{\pi-d_1}{2\pi} \mathbf{a}_1^* - \frac{\pi-d_2}{2\pi} \mathbf{a}_2^* \end{aligned} \quad (50)$$

with

$$\begin{aligned} d_1 &= \text{Re} \left[ \arccos \left( \frac{t_3^2 + t_2^2 - t_1^2}{2t_2t_3} \right) \right] \\ d_2 &= \text{Re} \left[ \arccos \left( \frac{t_3^2 + t_1^2 - t_2^2}{2t_1t_3} \right) \right], \end{aligned} \quad (51)$$

where  $\text{Re}(x)$  takes the real part of  $x$ . The cartesian coordinates of the Dirac points  $\mathbf{D}^{(\prime)} = (D_x^{(\prime)}, D_y^{(\prime)})$  are given by

$$\begin{aligned} \mathbf{D} &= \left( (d_1 + d_2 - 2\pi)/a_0, (d_1 - d_2)/\sqrt{3}a_0 \right) \\ \mathbf{D}' &= \left( (-d_1 - d_2 + 2\pi)/a_0, (d_2 - d_1)/\sqrt{3}a_0 \right). \end{aligned} \quad (52)$$

Then, since the Dirac points  $\mathbf{D}^{(\prime)}$  are not located anymore at the corner  $\mathbf{K}^{(\prime)}$  of the Brillouin zone, the range  $\Delta k_{\parallel}$  of existence of edge states is modified as:

$$\Delta k_{\parallel} = |\mathbf{D} - \mathbf{D}'| |\sin(\theta + \beta)| \quad (53)$$

where  $\beta$  is the angle between the line  $[\mathbf{D}'\mathbf{D}]$  and the  $k_x$  axis (see Fig. 17), which is then given by

$$\begin{aligned} \cos \beta &= 2 \frac{2\pi/a_0 - D'_x}{|\mathbf{D} - \mathbf{D}'|}, \\ \sin \beta &= 2 \frac{D'_y}{|\mathbf{D} - \mathbf{D}'|}. \end{aligned} \quad (54)$$

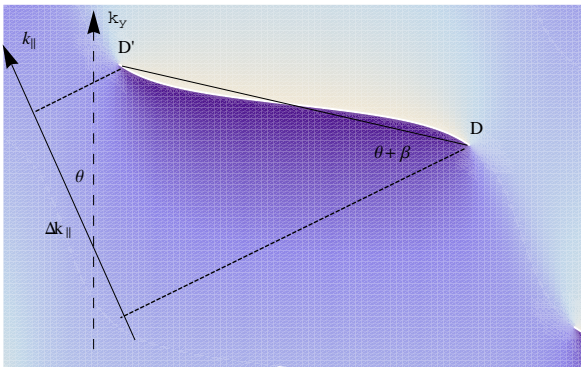


FIG. 17. Projection of the discontinuity line of  $\tilde{\phi}(\mathbf{k})$  onto the  $k_{\parallel}$  axis. The asymmetry of the hopping induces a modification of the discontinuity locations as compared with Fig. 14.

Using Eqs. (30) and (54), the range for the edge states reads:

$$\Delta k_{\parallel} = \frac{\left| (n-m) \left( \frac{2\pi}{a_0} - D'_x \right) + \sqrt{3} (n+m) D'_y \right|}{\sqrt{n^2 + m^2 + mn}}. \quad (55)$$

Next, by using the expression of the positions  $D'_x$  and  $D'_y$  given in (52) one finds:

$$\Delta k_{\parallel} = \frac{2 |nd_2 - md_1|}{a_0 \sqrt{n^2 + m^2 + nm}} \quad (56)$$

as well as

$$\mathcal{R} = \frac{|nd_2 - md_1|}{\pi}, \quad (57)$$

where  $d_1$  and  $d_2$  are given by Eqs. (51). These results give a criteria for the existence of edge states that links the anisotropy of the hopping parameters encoded in  $d_1$  and  $d_2$  with the nature of the edge characterized by  $(m, n)$ . In the isotropic case, we have  $d_1 = d_2 = \pi/3$ , and we recover the result (47) discussed in the previous section. The formula (56) means that an edge state exists in graphene-like structures if  $|nd_1 - md_2| \neq 0$ .

An interesting consequence is that, for a given type of ribbon, edge states can emerge or collapse when an anisotropy is applied. For instance, edge states can emerge for armchair-like boundary conditions ( $m = n$ ) when either  $t_1/t_3 \neq 1$  or  $t_2/t_3 \neq 1$  (see Refs. [25] and [33] for the case  $n = m = 1$ ). This is clearly displayed in Fig. 18. In the same way, edge states can collapse by manipulating the asymmetry of the hopping in such a way that  $|nd_1 - md_2| = 0$ .

### B. Merging of Dirac points and edge states

As one increases the anisotropy of the system, for instance by modifying one of the ratio  $t_i/t_j$ , one may eventually reach a point where  $t_1 = t_2 + t_3$  (or the equivalent up to a cyclic permutation of the indices). From Eq. (51), this condition implies that  $d_1$  and  $d_2$  take the values 0 or  $\pi$ , which, from Eq. (52), corresponds to a *merging of the Dirac points*. By increasing further the anisotropy, a gap opens at the merging point. This merging is a topological transition since the Berry phases  $\pm\pi$  associated to the two Dirac points annihilate at the transition.<sup>30,32</sup>

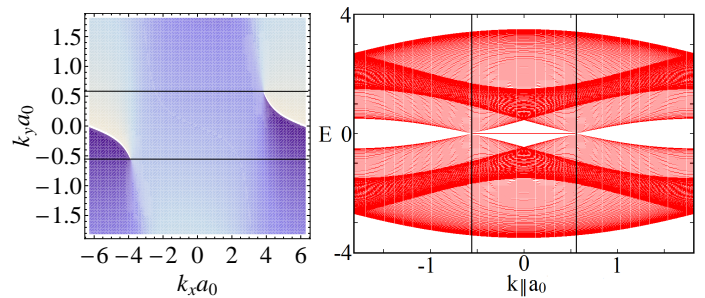


FIG. 18. (Left) Density plot of the phase  $\tilde{\phi}(\mathbf{k})$  for  $t_1 = 1$ ,  $t_2 = 1.5$  and  $t_3 = 1$  represented in the Brillouin zone corresponding to armchair edges. The two horizontal lines delimit the region where  $\mathcal{Z}(k_{\parallel}) = \pi$ . (Right) Band structure of an armchair ribbon with the same hopping parameters. In this case,  $k_{\parallel} = k_y$ . The two vertical lines delimit the same range as in the left panel, which is such that edge states at zero energy, clearly separated from the bulk bands, have emerged.

This topological transition is a bulk property, and is thus independent of the orientation of the anisotropy. On the other hand, the existence of edge states at the merging transition and beyond depends on the orientation of the ribbon with respect to this anisotropy, and this information is still contained in the Zak phase. Indeed the anisotropy of the hopping parameters controls the size and the location of the lines of discontinuities of  $\tilde{\phi}(\mathbf{k})$ . It is therefore essential to distinguish which pair of Dirac points merges. There are three possibilities :

- $t_3 \geq t_1 + t_2$

In this configuration, the Dirac points that merge are the endpoints of the same discontinuity line. Then, the discontinuities disappear at the merging ( $t_1 + t_2 = t_3$ ) and the Zak phase vanishes. This leads to

$$\mathcal{R} = 0 \quad (58)$$

whatever  $m$  and  $n$  (see top panel of Fig. 19), implying that edge states never exist in this case. As an illustration, we plot in Fig. 19 the band structure of a zigzag ribbon exactly at the merging point: the zero energy edge-states<sup>2</sup> of the isotropic case have collapsed because the Zak phase is zero for all  $k_{\parallel}$ .

The situation is totally different when the two merging Dirac points are attached to two distinct discontinuity lines, which occurs when  $t_1 - t_2 = \pm t_3$ . In this case, the two discontinuity-lines themselves merge, implying that  $\mathcal{R}$  is an integer, as we discuss now.

- $t_1 \geq t_2 + t_3$

In this case we have  $d_2 = 0$  and  $d_1 = \pi$ , which leads to

$$\mathcal{R} = |m| \quad (59)$$

for all  $n$ . For instance, there is no edge state for zigzag edge at  $\theta = +\pi/6$  (see center panels of Fig. 19), but there is one over the whole ribbon Brillouin zone for armchair edges and for zigzag edges at  $\theta = -\pi/6$ . We notice that the existence of edge states now only depends on the orientation of the edge given by  $\theta$  but not on  $k_{\parallel}$  anymore.

- $t_2 \geq t_1 + t_3$

In this case  $d_1 = 0$  and  $d_2 = \pi$  and we find

$$\mathcal{R} = |n| \quad (60)$$

whatever the value of  $m$ . Of course this case is equivalent to the one discussed previously with the substitution  $m \leftrightarrow n$  that is  $\theta \rightarrow -\theta$ . The phase  $\tilde{\phi}(\mathbf{k})$  and the corresponding band structure for zigzag ribbons at  $\theta = +\pi/6$  are represented in Fig. 19 (bottom panels).

In summary, we note that in all three cases, at the merging, the Zak phase becomes independent of  $k_{\parallel}$  and remains unchanged in the gapped phase. This implies that at the merging transition and beyond,  $\mathcal{R}$  is necessarily an integer. This is obvious from Figs. 19 : the merging of the Dirac points implies either a disparition of the discontinuity lines or their transformation into an infinite line.

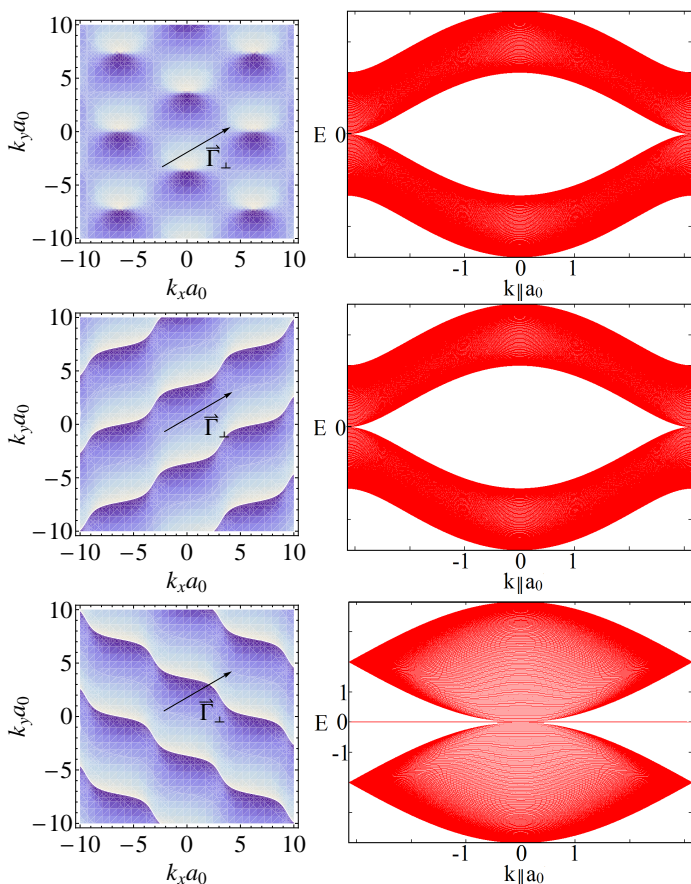


FIG. 19. Density plot of the phases  $\tilde{\phi}(\mathbf{k})$  at the merging of the Dirac points, and band structure for zigzag ribbon with  $\theta = \pi/6$  (that is  $\mathbf{T}(m=0, n=1) \rightarrow \Gamma_{\perp}(m=0, n=1) = (1, 0)$ ). (Top)  $t_1 = 1$ ,  $t_2 = 1$  and  $t_3 = 2$ , (center)  $t_1 = 2$ ,  $t_2 = 1$  and  $t_3 = 1$ , (bottom)  $t_1 = 1$ ,  $t_2 = 2$  and  $t_3 = 1$ . The scale is given in units of  $1/a_0$ .

## V. CONCLUSION

In this paper, we have investigated the correspondence between the Zak phase and the existence of edge states for arbitrarily oriented graphene ribbons with a large class of edge shapes. We have proposed a definite prescription to

compute the Zak phase in order to predict the number of edge states. The approach we have developed consists in constructing the appropriate 2D Brillouin zone associated with the vector  $\mathbf{T}(m, n)$  which defines the edge. The Zak phase  $\mathcal{Z}(k_{\parallel})$  giving the number of edge states for each  $k_{\parallel}$  is then directly obtained by integrating the Berry connection along a path fixed by  $\mathbf{T}(m, n)$  and  $k_{\parallel}$  in this 2D Brillouin zone.

We stress that this bulk-edge correspondence is, beyond the 1D chain of dimers case, only rigorously proven here for zigzag edges. It is therefore so far a conjecture for the class of edges we have defined. This conjecture is however supported by the fact that it reproduces all the known previous results obtained (numerically or otherwise) in the literature for various specific types of edges.<sup>2,3,14,20-22</sup>

In practice, the value of the integral defining the Zak phase is easily obtained graphically. Our approach therefore does not require any sophisticated formalism or calculation, and gives an elegant understanding of the origin of the edge-dependent edge states in terms of a topological bulk quantity. In particular, it provides a simple understanding of the appearance and disappearance of edge states by manipulating the anisotropy of the tight-binding hopping parameters. Such a manipulation may be induced in graphene by applying an uniaxial stress or bending of the sheet,<sup>34</sup> or in photonic crystals which mimic the same physics, by changing the distance between the confining mirrors.<sup>6</sup>

We finish with a few comments concerning the connection between Zak phase and edge states.

First, this bulk-edge correspondence differ from the ones in quantum Hall systems<sup>35-38</sup> or  $\mathbb{Z}_2$  topological insulators<sup>38,39</sup> since here the existence of edge states precisely depends on the orientation of the edge. This difference with the usual bulk topological numbers originates from the fact that the Zak phase is a 1D (rather than 2D) integral of the Berry connection.

Second, we stress that within our approach, the vector  $\mathbf{T}(m, n)$  defining the periodicity of the ribbon entirely determine the Zak phase. As many different shapes may correspond to the same vector  $\mathbf{T}(m, n)$ , the Zak phase and therefore the number of edge states are expected to be independent of the variation of the edge geometries as long as they correspond to the same  $\mathbf{T}(m, n)$ .<sup>40</sup>

Finally, our description of edge states in terms of the Zak phase is a priori not restricted to graphene but should be in principle also applicable to other 2D systems like d-wave superconductors,<sup>14</sup> square lattice with half a quantum flux per unit cell<sup>33</sup> or bi-layer graphene<sup>17</sup> for instance.

*Acknowledgments* - We acknowledge useful discussions with J.-N Fuchs, M. Büttiker, J. Li, C. Bena and L. Bileanu. This work is supported by the NANOSIMGRAPHENE Project No. ANR-09-NANO-016-01 of ANR/P3N2009. In Geneva P. D. was supported by the European Marie Curie ITN NanoCTM.

## Appendix A: Construction of the Brillouin zone

In this appendix, we give a brief reminder of the reason why the vectors  $\Gamma_{\parallel}$  and  $\Gamma_{\perp}$  defined by Eqs. (31)-(32) actually generate a Brillouin zone when  $n$  and  $m$  are coprime integers.

This latter condition indeed implies that one can find two integers  $(m', n')$  such that  $mn' - nm' = 1$ , in which case the

couple of vector  $(\mathbf{T}, \mathbf{N})$ , with  $\mathbf{N} = m'\mathbf{a}_1 + n'\mathbf{a}_2$ , form a basis of the Bravais lattice. The choice of  $(m', n')$ , and thus of  $\mathbf{N}$ , is not unique, but this is irrelevant for our purpose.

From  $(\mathbf{T}, \mathbf{N})$ , one deduce a basis  $(\mathbf{\Gamma}_N, \mathbf{\Gamma}_\perp)$  of the reciprocal lattice,

$$\mathbf{\Gamma}_N = n'\mathbf{a}_1^* - m'\mathbf{a}_2^*, \quad (\text{A1})$$

$$\mathbf{\Gamma}_\perp = n\mathbf{a}_1^* - m\mathbf{a}_2^*, \quad (\text{A2})$$

which is such that  $\mathbf{\Gamma}_\perp \perp \mathbf{T}$ . A Brillouin zone can thus be ob-

tained from the parallelogram generated by  $(\mathbf{\Gamma}_N, \mathbf{\Gamma}_\perp)$ . More generally however, any vector  $\mathbf{\Gamma}$  such that  $(\mathbf{\Gamma} - \mathbf{\Gamma}_N) \parallel \mathbf{\Gamma}_\perp$  is such that the parallelogram generated by  $(\mathbf{\Gamma}, \mathbf{\Gamma}_\perp)$  is a Brillouin zone. A natural choice is to take for  $\mathbf{\Gamma}$  the vector  $\mathbf{\Gamma}_\parallel$  which is parallel to  $\mathbf{T}$  (and thus orthogonal to  $\mathbf{\Gamma}_\perp$ ). Since  $\mathbf{T} \cdot \mathbf{\Gamma}_N = 2\pi(mn' - nm') = 2\pi$ , one has  $|\mathbf{\Gamma}_\parallel| = 2\pi/|\mathbf{T}|$  which is nothing but the size of the (1D) Brillouin zone of the ribbon.

- 
- <sup>1</sup> A. Geim and K. Novoselov, The rise of graphene, *Nature materials* **6**, 183 (2007).
- <sup>2</sup> M. Fujita, K. Wakabayashi, K. Nakada, and K. Kusakabe, Peculiar localized state at zigzag graphite edge, *J. Phys. Soc. Jpn* **65**, 1920 (1996).
- <sup>3</sup> K. Nakada, M. Fujita, G. Dresselhaus, and M. S. Dresselhaus, Edge state in graphene ribbons: Nanometer size effect and edge shape dependence, *Phys. Rev. B* **54**, 17954 (1996).
- <sup>4</sup> Y. Kobayashi, K. I. Fului, T. Enoki, K. Kusakabe, and Y. Kaburagi, Observation of zigzag and armchair edges of graphite using scanning tunneling microscopy and spectroscopy, *Phys. Rev. B* **71**, 193406 (2005).
- <sup>5</sup> Y. Niimi, T. Matsui, H. Kambara, K. Tagami, M. Tsukada, and H. Fukuyama, Scanning tunneling microscopy and spectroscopy of the electronic local density of states of graphite surfaces near monoatomic step edges, *Phys. Rev. B* **73**, 085421 (2006).
- <sup>6</sup> U. Kuhl, S. Barkhofen, T. Tudorovskiy, H.-J. Stockmann, T. Hossain, L. de Forges de Parny, and F. Mortessagne, Dirac point and edge states in a microwave realisation of tight-binding graphene-like structures, *Phys. Rev. B* **82**, 094308 (2010).
- <sup>7</sup> Y.-W. Son, M. L. Cohen, and S. G. Louie, Half-metallic graphene nanoribbons, *Nature* **444**, 347 (2006).
- <sup>8</sup> O. V. Yazyev and M. I. Katsnelson, Magnetic correlations at graphene edges: Basis for novel spintronics devices, *Phys. Rev. Lett* **100**, 047209 (2008).
- <sup>9</sup> B. I. Halperin, Quantized Hall conductance, current-carrying edge states, and the existence of extended states in a two-dimensional disordered potential, *Phys. Rev. B* **25**, 2189 (1982).
- <sup>10</sup> M. Büttiker, Absence of backscattering in the quantum Hall effect in multiprobe conductors, *Phys. Rev. B* **38**, 9375 (1988).
- <sup>11</sup> B. A. Bernevig, T. A. Hughes, and S.-C. Zhang, Quantum spin Hall effect and topological phase transition in HgTe quantum wells, *Science* **314**, 1757 (2006).
- <sup>12</sup> M. König, H. Buhmann, L. W. Molenkamp, T. Hughes, C.-X. Liu, X.-L. Qi, and S.-C. Zhang, The quantum spin Hall effect: theory and experiment, *J. Phys. Soc. Jpn* **77**, 031007 (2008).
- <sup>13</sup> D. J. Thouless, M. Kohmoto, M. P. Nightingale, and M. den Nij, Quantized Hall conductance in a two-dimensional periodic potential, *Phys. Rev. Lett.* **49**, 405 (1982).
- <sup>14</sup> S. Ryu and Y. Hatsugai, Topological origin of zero-energy edge states in particule-hole symmetric systems, *Phys. Rev. Lett.* **89**, 077002 (2002).
- <sup>15</sup> R. Mong and V. Shivamoggi, Edge states and the bulk-boundary correspondence in Dirac Hamiltonians, *Phys. Rev. B* **83**, 125109 (2011).
- <sup>16</sup> K. Sasaki, K. Wakabayashi, and T. Enoki, Berry's Phase for Standing Wave Near Graphene Edge, *New J. Phys.* **12**, 083023 (2010).
- <sup>17</sup> J. Li, A. F. Morpurgo, M. Büttiker, and I. Martin, Marginality of bulk-edge correspondence for single-valley Hamiltonians, *Phys. Rev. B* **82**, 245404 (2010).
- <sup>18</sup> D. J. Klein and L. Bytautas, Graphitic edges and unpaired  $\pi$ -electron spins, *J. Phys. Chem. A* **103**, 5196 (1999).
- <sup>19</sup> Z. Liu, K. Suenaga, P. J. F. Harris, and S. Iijima, Open and closed edges of graphene layers, *Phys. Rev. Lett.* **102**, 015501 (2009).
- <sup>20</sup> K. Wakabayashi, Y. Takane, M. Yamamoto, and M. Sigrist, Edge effect on electronic transport properties of graphene nanoribbons and presence of perfectly conducting channel, *Carbon* **47**, 124 (2009).
- <sup>21</sup> K. Wakabayashi, S. Okada, R. Tomita, S. Fujimoto, and Y. Natsume, Edge states and flat bands of graphene nanoribbons with edge modifications, *J. Phys. Soc. Jpn.* **79**, 034706 (2010).
- <sup>22</sup> W. Jaskolski, A. Ayuela, M. Pelc, H. Santos, and L. Chico, Edge states and flat bands in graphene nanoribbons with arbitrary geometries, arXiv:1104.0147v1 (2011).
- <sup>23</sup> A. R. Akhmerov and C. W. J. Beenakker, Boundary conditions for Dirac fermions on a terminated honeycomb lattice, *Phys. Rev. B* **77**, 085423 (2008).
- <sup>24</sup> J. Zak, Berry's phase for energy bands in solids, *Phys. Rev. Lett.* **62**, 2747 (1988).
- <sup>25</sup> H. Dahal, Z. Hu, N. Sinitsyn, K. Yang, and A. Balatsky, Edge states in a honeycomb lattice: effects of anisotropic hopping and mixed edges, *Phys. Rev. B* **81**, 155406 (2010).
- <sup>26</sup> When  $M$  is finite, there is a finite range of parameters  $1 - 1/(M + 1) < t'/t < 1$ , for which there are no edge states ( $M$  bulk states), although the Zak phase is  $\pi$ .
- <sup>27</sup> The energy of the edge states is zero only when the width of the system is larger than the localization length, otherwise the edge states at each edge hybridize and the resulting energy is not zero.
- <sup>28</sup> J. Cai, P. Ruffieux, R. Jaafar, M. Bieri, T. Braun, S. Blankenburg, M. Muoth, A. Seitsonen, M. Saleh, X. Feng, K. Mullen, and R. Fasel, Atomically precise bottom-up fabrication of graphene nanoribbons, *Nature Letters* **466**, 470 (2010).
- <sup>29</sup> Y. Hasegawa, R. Konno, H. Nakano, and M. Kohmoto, Zero modes of tight-binding electrons on the honeycomb lattice, *Phys. Rev. B* **74**, 033413 (2006).
- <sup>30</sup> P. Dietl, F. Piéchon, and G. Montambaux, New magnetic field dependance of Landau levels in graphenelike structure, *Phys. Rev. Lett.* **100**, 236405 (2008).
- <sup>31</sup> B. Wunsch, F. Guinea, and F. Sols, Dirac-point engineering and topological phase transitions in honeycomb optical lattices, *New J. Phys.* **10**, 103027 (2008).
- <sup>32</sup> G. Montambaux, F. Piéchon, J.-N. Fuchs, and M.-O. Goerbig, A universal Hamiltonian for motion and merging of Dirac points in a two-dimensional crystal, *Eur. Phys. J. B.* **72**, 509 (2009).
- <sup>33</sup> P. Delplace, *États de bords et cônes de Dirac dans des cristaux bidimensionnels*, PhD thesis. Université Paris-Sud XI, 2010.
- <sup>34</sup> L. Pauling, *Proc. N. A. S.* **56**, 1646 (1966).
- <sup>35</sup> Y. Hatsugai, Edge states in the integer quantum Hall effect and the Riemann surface of the Bloch function, *Phys. Rev. B* **48**, 11851 (1993).

- <sup>36</sup> Y. Hatsugai, Chern number and edge states in the integer quantum Hall effect, *Phys. Rev. Lett.* **71**, 3697 (1993).
- <sup>37</sup> N. Hao, P. Zhang, Z. Wang, W. Zhang, and Y. Wang, Topological edge states and quantum Hall effect in the Haldane model, *Phys. Rev. B* **78**, 075438 (2008).
- <sup>38</sup> X.-L. Qi, Y.-S. Wu, and S.-C. Zhang, General theorem relating the bulk topological number to edge states in two-dimensional insulators, *Phys. Rev. B* **74**, 045125 (2006).
- <sup>39</sup> Z. Wang, N. Hao, and P. Zhang, Topological winding properties of spin edge states in Kane-Mele graphene model, *Phys. Rev. B* **80**, 115420 (2009).
- <sup>40</sup> Preliminary numerical results seem to confirm this prediction, (L. Bilteanu and C. Bena, Private communication).